Multiphysics modelling of photo-polymerization in stereolithography printing process and validation

K. Gao, B.L.J. Ingenhut, A.P.A. van de Ven, F.O. Valega Mackenzie, A.T. ten Cate

Brightlands Materials Center, Urmonderbaan 22, 6167 RD, Geleen, The Netherlands

TNO Materials Solutions, High Tech Campus 25, 5656 AE, Eindhoven, The Netherlands

Introduction

Additive Manufacturing (AM) has become an attractive and ubiquitous technology in rapid prototyping but also in the biomedical realm such as in dental and hearing aid applications. The adoption is mainly due to its free form flexibility and cost reduction during the manufacturing process [1,2]. Stereolithography (SLA), a type of AM technology based on photo-curable resins, is ideal for rapid prototyping because it can achieve substantially high printing resolution (in the order of 10μm) when compared to other AM technologies in addition to higher printing speeds. Despite these advantages, problems in the printed geometries, such as warpage, are always critical for the quality of the finalized products. A major source of the warpage is due to the material inhomogeneity induced by the printing process conditions [2]. To understand and control the warpage, a process model is necessary to simulate the photo-polymerization reaction which is an essential part of SLA. Moreover, in application, it is important to understand how process conditions, such as the exposure time and the layer thickness, influence mechanical properties of photo-polymers and final products. Furthermore, a numerical model linking process conditions and material properties is an essential part of industry digitalization.

Recently, several models have been developed to investigate the relation of the process and the properties of the material [3,4,5]. Due to the complexity of these models, many parameters, particularly on mechanical properties of the polymer, have to be obtained by sophisticated experiments. Moreover, the computational cost of simulating a multi-layer product is usually high since these models contain highly nonlinear material behaviors. Therefore, this paper focuses on developing a relatively simple multiphysics model of the photo-polymerization process. This model can be used to find out the relation of the process conditions and the resulting properties of printed parts, e.g. warpage. The required parameters in the model are measured by commercial devices with simple modifications. Moreover, the computational cost of the model has been taken into account so that a multi-layer product can be simulated. In the following section, the governing equations of the model will be given. Then, the layer-by-layer printing process is described. Afterwards, the characterization methods and the experimental results are discussed. In the end, the model is validated by comparing with new experiments.

Governing equations

Governing equations of the model are presented in this section. It includes a chemical kinetics model and a classical thermo-mechanical model.

Photo-polymerization kinetics

The polymerization process contains three basic stages: initiation, propagation and termination. A review [6] is recommended for the readers. Besides, various models has been developed and more details on these models can be found in the review [7]. In this paper, the kinetics model is based on Goodner and Bowman's work [8]. By assuming that the free radicals are reacted immediately, the polymerization rate is described as the consumption of the monomer

$$\frac{\partial[\mathrm{M}]}{\partial t} = -R_p = -k_p[\mathrm{M}]\sqrt{\frac{R_i}{2k_t}}\ , \qquad (1.1)$$

where [M]([mol/m^3]) is the concentration of the monomer, k_p is a propagation parameter and k_t is a termination parameter. The rate of initiation depends on the concentration of the photo-initiator:

$$R_i = 2\phi\epsilon_{\mathrm{PI}}[\mathrm{PI}]I, \qquad (1.2)$$

where ϕ ([-]) is the quantum yield of the photo-initiator, ϵ_{PI} ([m^2/mol]) is the molar extinction coefficient of the photo-initiator and [PI] ([mol/m^3]) is the molar concentration of the photo-initiator. The double-bond conversion p ([-]) is defined as the change of the monomer concentration:

$$p = 1 - \frac{[\mathrm{M}]}{[\mathrm{M}]_0}\ . \qquad (1.3)$$

In this paper, the conversion always means the double-bond conversion. In the propagation and the termination processes, two critical free volume fractions are introduced to indicate if the reaction is reaction-limited or diffusion-limited [8]: when the free volume (depending on the conversion and the

temperature) is lower than the critical volume, the diffusion of the free radicals or the long polymer chains becomes more difficult in the material and it is the limiting factor of the polymerization rate. Generally, the termination becomes diffusion-limited at an early stage, when the conversion is as low as 5% [7], because of the large polymer chain. Because the low-conversion stage is not the interest of this paper, the termination process is assumed to be diffusion-limited during the whole process. Moreover, when the propagation becomes diffusion-limited, effects of the monomer concentration can be ignored. Based on the above discussion, an equation is derived:

$$R_p = \frac{C_0 \exp\left(-\frac{E_{Rp}}{RT}\right)}{1+\exp\left(\frac{1}{f}-\frac{1}{f_{c,p}}\right)}[\mathrm{M}]\sqrt{I}. \quad (1.4)$$

Here, the constant C_0 depends on the monomer. The activation energy is E_{Rp} ([J/mol]) and $f_{c,p}$ is the critical free volume of the propagation. These three parameters should be characterized by experiments. The light absorption follows Beer-Lambert law

$$\frac{\partial I}{\partial z} = \frac{I}{D_p} \quad \text{if} \quad z \le z_0. \quad (1.5)$$

Here, the light direction is pointing to -z direction and z_0 is the position of the surface where the light is projected. Moreover, D_p ([m]) is the light penetration depth. When the photo-initiator is the only light absorber in the resin, the light penetration depth is written as[1]

$$D_p = \frac{1}{\epsilon_{\mathrm{PI}}[\mathrm{PI}]_0 \ln 10}, \quad (1.6)$$

where ϵ_{PI} is the extinction coefficient of the photo-initiator. In practice, a dye can be added which might influence on the formulation slightly. More importantly, it allows for a higher controlled resolution in the layer thickness. In this case the light penetration depth is expressed as

$$D_p = \frac{1}{\left(\epsilon_{\mathrm{PI}}[\mathrm{PI}]_0 + \epsilon_{\mathrm{dye}}[\mathrm{dye}]_0\right)\ln 10}. \quad (1.7)$$

Thermo-mechanics

The photo-polymerization of acrylic monomers is generally an exothermic process. The absorption of the UV light also increases the temperature. Then, energy conservation is written as

$$\rho C_p \frac{\partial T}{\partial t} + \vec{\nabla}\cdot\left(-k\vec{\nabla}T\right) = R_p \Delta H + \left(\epsilon_{\mathrm{PI}}[\mathrm{PI}] + \epsilon_{\mathrm{dye}}[\mathrm{dye}]\right) I, \quad (1.8)$$

where ρ ([kg/m^3]) is the density of the material, C_p ([J/(kg·K)]) is the heat capacity at constant pressure, k ([W/(m·K)]) is the thermal conductivity and ΔH ([J/mol]) is the enthalpy change of the polymerization. On the other hand, momentum conservation gives

$$\rho\frac{\partial \vec{u}}{\partial t} + \vec{\nabla}\cdot\underline{\underline{\sigma}}^{\mathrm{T}} = \vec{0}, \quad (1.9)$$

where $\vec{u}$ ([m]) is the displacement and $\underline{\underline{\sigma}}$ ([Pa]) is Cauchy's stress. The stress-strain relation of the material will be discussed later. The polymerization contributes two types of strains: a thermal expansion due to the temperature change and a chemical shrinkage because of the conversion. The chemical shrinkage is assumed to be isotropic and linearly depends on the conversion, i.e.

$$\epsilon^{\mathrm{chem}} = -p\epsilon^{\mathrm{chem}}_{\mathrm{max}}, \quad (1.10)$$

where $\epsilon^{\mathrm{chem}}_{\mathrm{max}}$ ([-]) is the maximum chemical shrinkage when the monomer is fully converted into the polymer. A mixture relation is assumed for the density, the heat capacity, the thermal conductivity and the coefficient of thermal expansion (CTE):

$$\chi = (1-p)\chi_{\mathrm{mono}} + p\chi_{\mathrm{poly}} \quad \text{with} \quad \chi = \rho, \rho C_p, k, \alpha. \quad (1.11)$$

Simulation of the SLA process

In this work, the printing process of a Digital Light Projection (DLP) printer (Rapidshape S60) is simulated: in the beginning, the 3D geometry of the product is sliced into a series of 2D images with a specified layer thickness along the printing direction. Then, a box of the resin is placed in the printer and the printing can start. During the printing of one layer, the UV light with the corresponding 2D image pattern is projected on the surface of the resin with a given exposure time. The liquid resin exposed to the UV-light will become solid and connected with the previous printed solid layers. After the period of the layer exposure time, the light is off and the position of the solid layers is changed so that the new liquid resin can fill-in and cover the newly-printed solid layer for a next printing. When all layers are printed, the product will be removed from the printing box and the residual liquid resin needs to be washed away carefully. In practice, a post-curing process will follow to ensure additional solidification of the

[1] This definition is slightly different from some literature. For example, there is also 2 in the denominator in [9].

product. However, the post-curing process is not considered in this paper.

To simulate the printing process, the developed multiphysics model is implemented in COMSOL Multiphysics© (ver. 5.3a). An Ordinary Differential Equation (ODE) module and a Partial Differential Equation (PDE) module are used to solve Eq. (1.1) and Eq. (1.5) respectively. Eq. (1.8) and (1.9) are solved together by using Structural Mechanics and Heat Transfer modules. To achieve the layer-by-layer printing, the element size along the printing direction should not exceed the layer thickness. An empty material (with a Young's modulus of 10^{-12} Pa and a zero thermal conductivity) is also used when the layer is not printed yet. In the beginning of the simulation, all layers are set as the empty material. When the printing starts, the material of the first layer is switched to the monomer. The light with a given pattern is positioned on the surface of the first layer. After the layer exposure time, the position of the UV light is shifted to the surface of the second layer immediately and the light pattern will be adjusted to the corresponding one. Then, the printing of the second layer starts and so it is with remaining layers. Therefore, all intermediate processes like filling of the new liquid resin are not considered. For the boundary conditions, the top and the back surfaces of the printed layers are fixed and thermal-isolated conditions are adopted on all external surfaces. After the printing, the constraints on the surfaces are removed and the temperature of the external surfaces are set to 20 °C.

Material characterization

Most parameters necessitated in our model have to be obtained through measurements. A general workflow is described in this section. In this paper, ethoxylated(4) bisphenol a dimethacrylate(98wt%, Sartomer SR540) has been chosen and the photo-initiator is bis(2,4,6-trimethylbenzoyl) phenyl phosphoinositide (2wt%, Omnirad 819).

Photo-polymerization kinetics

Since no dye is added to the resin, the photo-initiator is the only light-absorbing entity in the resin, i.e. Eq. (1.6) is used. In the beginning of the photo-polymerization process, the diffusion of the monomer is not the limiting factor of the reaction. Therefore, the reaction rate in Eq. (1.4) can be approximated to be a constant. Assume that the diffusion of the monomer becomes the limiting factor when the material transits from the fluid to the solid (defined as the gel point). In this case, the thickness of the solid layer h is related to the constant C_0 and the light penetration depth D_p

$$h = 2D_p \ln\left(\frac{t}{t_{cri}}\right), \qquad (1.12)$$

where t_{cri} is the required exposure time for the material to reach the gel point. Hence, to measure the light penetration depth, a series of single layer samples are printed with various exposure times in the 3D printer and the printed thickness are measured afterwards. Then, D_p is obtained by fitting Eq. (1.12) with the measured data as shown in Figure 1.

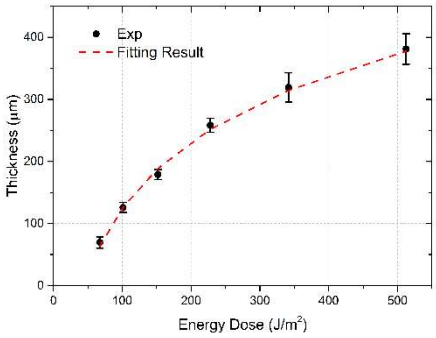

Figure 1 Layer thickness test of the material in the 3D printer and the fitting result of Eq. (1.12).

The conversion can be measured by the Attenuated Total Reflectance (ATR) technique with a Fourier-Transform Infrared Spectroscopy (FTIR). In this work, a special sample holder as illustrated in Figure 2 is made between the FTIR (Thermofischer Nicolet 6700 series) and the UV source (LED engine LZC-00UA00 400 centered at 405 nm) so that the in-situ conversion can be monitored during the photo-polymerization process. The measurement area is purged with N_2 to prevent oxygen inhibition.

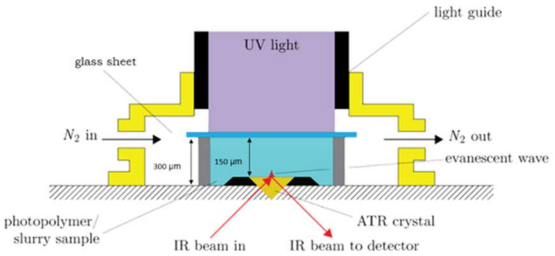

Figure 2 Illustration of the sample holder used in the FTIR measurement.

In this measurement, the room temperature is kept at 20°C and the variation of the temperature in the holder is ignored. Seven samples are measured in total. The light intensity along the light direction is calculated by Eq. (1.5) based on the obtained light penetration depth. According to Eq. (1.4), the average conversion is plotted against the product of the time and the square root of the light intensity in Figure 3. The critical free volume $f_{c,p}$ and the

kinetics constant $C_0 \exp\left(-\frac{E_{Rp}}{RT}\right)$ at room temperature can be determined by fitting the data. The result of the model is also given in Figure 3, showing a good agreement with the experiment.

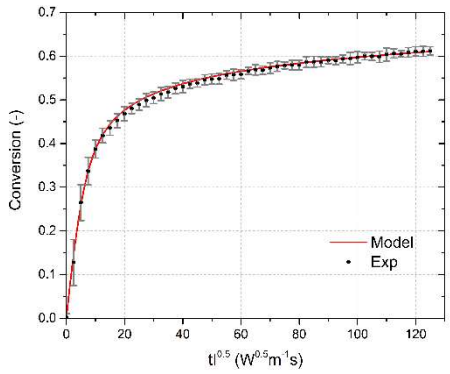

Figure 3 In-situ conversion measurement during the reaction and the fitting result of the kinetics model. The error bars stand for the standard deviations of 7 samples.

Mechanical properties

For an isotropic linear elastic material, two parameters are required: the shear modulus and the Poisson's ratio. In this work, the Poisson's ratio is assumed as 0.4 and a phenomenological correlation of the conversion and the storage shear modulus is adopted

$$G = G_{\text{mono}} + \frac{G_{\text{poly}}}{1+\exp\left[-\kappa(p-p_{half})\right]}, \quad (1.13)$$

where G_{mono} the shear modulus of the monomer, G_{poly} the one of the polymer. The half-conversion p_{half} is the one when the shear modulus of the material is a half of G_{poly}. The positive parameter κ is a shape control parameter.

The shear modulus is measured by a rheometer (Anton Paar MCR 302) connected with the UV source (LED engine LZC-00UA00 400 centered at 405 nm). The in-situ rheological behavior during the curing is recorded in the oscillation test. The storage shear modulus averaged from seven samples are plotted with respect to the time in Figure 4. The UV light is on from 30 s and the total exposure time is 210 s. The angular speed is 1 rad/s and the rotation amplitude is 0.01 rad. The solid curve presents the prediction of the correlation of Eq.(1.13) in which the parameters are obtained by assuming a constant thickness of 150 µm. As shown in Figure 4, in the first 30 s, the UV light is not on and the viscosity of the liquid resin was around 1-10 Pa·s. When the UV light is on, there is a sudden increase of the shear modulus because of the transition from the fluid to the solid in the polymerization process.

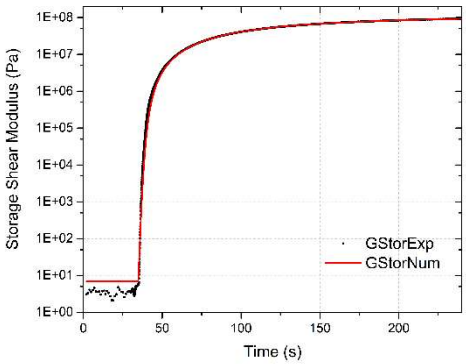

Figure 4 Measured storage shear modulus during the curing and the correlation of the conversion.

In the end of this section, the obtained parameters are summarized in Table 1. Other parameters required in the model are listed in Table 2.

Table 1 Parameters obtained in the characterization methods.

Parameter	Value
D_p	77.55[µm]
$f_{c,p}$	0.0382[-] (at 20ºC)
C_0	1.304[-]
E_{Rp}/R	2140[K]
G_{mono}	2.877[Pa]
G_{poly}	0.128[GPa]
κ	27.54[-]
p_{half}	0.628[-]

Validation

The developed model is validated by checking the conversion and the warpage of 50mm×5mm rectangle beams printed by the printer. The thickness of the beam is 1mm and the layer thickness is 0.1mm. According to the layer thickness test, the required exposure time of a layer with 0.1mm should be longer than 9s. Therefore, the exposure time per layer is set as 9.5s. According to Table 1, the light penetration depth is 77.55µm, showing that the previously-printed layers can be still influenced by the UV light. Therefore, the exposure time of the last layer (i.e. the 10th layer) is adjusted from 9.5s to 5 ×9.5s to study the influence of the exposure time. In the discussion, the 100% relative energy dose means that the last layer was printed in 9.5s and 500 % one has a exposure time of 5×9.5s. Besides, the first layer is printed with 1.5×9.5s to ensure a good adhesion between the first layer and the platform. In this paper, the light direction is pointing to the -z

direction. As illustrated in Figure 5, the back surface (z=0mm) means the one contacting with the platform of the printer. The front surface (z=1mm) presents the external surface of the 10th layer.

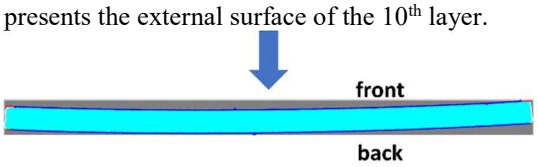

Figure 5 Illustration of the front surface, the back surface and the light direction. The beam shows a positive-bending shape and the image was processed by Matlab.

The conversion on the back surface is compared with the prediction of the model. Because the total thickness of the beam 1mm is much larger than D_p, the effective exposure time of the back surface in all samples are almost the same. Hence, there is no change of the conversion on the back surface, as supported in the model as shown in Figure 6. The measurement also agrees with the model quite well. The slight deviation of the model and the measurement may be due to the change of the light absorption abilities of the photo-initiator and the polymer.

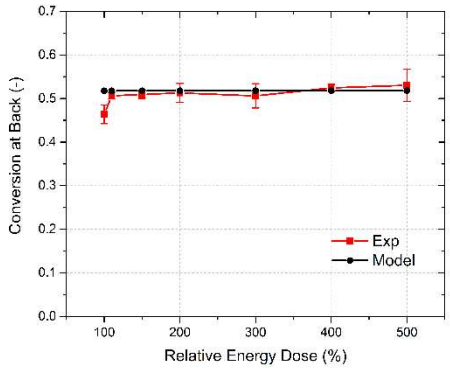

Figure 6 Comparison of the conversion on the back surface. The error bars are the standard deviations of seven samples.

On the other hand, the conversion on the front surface will increase with the exposure time, as shown in Figure 7. However, the experiment result is lower than the simulation consistently. There are several explanations: some free-radicals trapped in the polymer chains cannot be consumed immediately and it takes much longer time to consume these trapped radicals, i.e. the conversion will slightly increase after a sufficiently long period; the front surface is exposed to oxygen earlier than the back surface; some residual resin may remain on the front surface and it can have a significant influence on the FTIR measurement which measures a tiny amount of the material. Despite of the deviation, the increases of the conversion in the model and the experiment are quite close to each other.

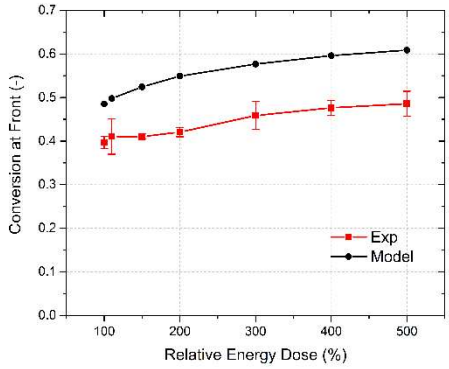

Figure 7 Comparison of the conversion on the front surface. The error bars are the standard deviations of seven samples.

Furthermore, the warpage of the printed samples is measured and compared with the model. In this paper, the warpage is quantified as the deflection of the beam. High-resolution (~3μm×3μm per pixel) pictures of the samples are taken by a digital camera (Nikon D90 and Nikon AF-D 200mm F/4.0 Micro IF ED Lens). By converting the images to binary ones, boundaries of the samples can be captured and fitting by fourth-order polynomials, as illustrated in Figure 5. The deflection of the back surface is defined as the difference of the displacement in the corner of the beam and the one in the middle. The experiment result is shown in Figure 8.

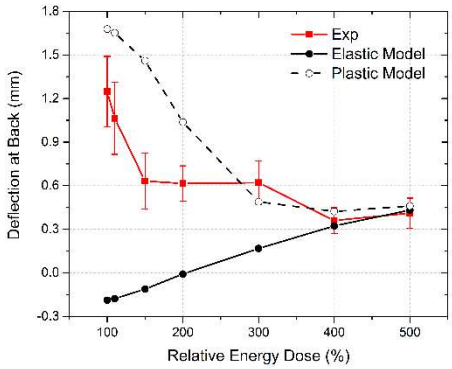

Figure 8 Comparison of the deflection of the back surface. The error bars are the standard deviations of seven samples.

When the material is purely elastic, the residual stress remaining in the beam is induced by the geometrical mismatch between layers with different conversion. As shown in Figure 6 and Figure 7, the conversion of the back surface is higher than the conversion of the front surface for 100% samples. Therefore, the back surface will shrink more than the front surface, suggesting a negative bending shape (i.e. a negative deflection). Similarly, for 500% samples, it shall have a positive deflection. As shown in Figure 8, the numerical result of the elastic model confirms this argument. However, the

experiment shows that the deflection of the beam is always positive and decreases significantly when the energy dose increases from 100% to 150%. Therefore, a purely elastic model is not sufficient to describe the residual stress in the beam.
Noting that the conversion can be as high as 50%, the corresponding chemical shrinkage can be around 1%, which already results in inelastic deformation for some polymers. To capture the generated residual stress during the printing, a plastic model is introduced by adding plasticity based on the elastic model. In the plastic model, the yielding stress of the material is assumed to be linearly proportional to the conversion before a transition value p_{tran} and becomes constant after that value. The values are given in Table 2. In Figure 8, it can be observed that the plastic model gives a much better prediction of the deflection: the deflection is always positive and has a significant decrease from 100% to 300%. Considering the large deviation of the samples from 100% to 300%, the plastic model shows a good agreement with the experiment.

Conclusions

In this paper, a workflow including a multiphysics model and material characterization methods was developed to investigate the effects of the photo-polymerization on SLA products. The model was implemented in COMSOL Multiphysics© and it involved a chemical reaction and a thermo-mechanical deformation. On the other hand, the kinetics parameters of the kinetics reaction were characterized by the in-situ measurement of the conversion. The storage shear modulus of the material was correlated to the conversion by monitoring the oscillation test in the UV-rheometer setup. In the end, the final conversion and the warpage of rectangular beams printed in the commercial 3D printer were compared with the prediction of the developed model. The comparison indicated that the residual stress developed throughout the printing process cannot be captured by a purely elastic material model. Nonlinear material models such as a plasticity model should be taken into account while predicting the warpage and mechanical properties of photo-polymers. This is a necessary feature to realistically simulate the behavior of printed parts using photo-curable resins.

Appendix

Table 2 Other parameters required for the model.

Parameter	Value
ρ_{mono}	1128[kg/m^3]
$T_{g,\text{mono}}$	213[K]
α_{mono}	200×10^{-6}[1/K]
k_{mono}	0.2[W/(m*K)]
$C_{p,\text{mono}}$	1190[J/(kg*K)]
ρ_{poly}	1200[kg/m^3]
$T_{g,\text{poly}}$	351.65[K]
α_{poly}	20×10^{-6}[1/K]
k_{poly}	0.2[W/(m*K)]
$C_{p,\text{poly}}$	1190[J/(kg*K)]
ΔH	79.95×10^3[J/mol]
$\epsilon_{\text{max}}^{\text{chem}}$	0.021[-]
$\overline{\sigma}_{\text{mono}}$	0.155[MPa]
$\overline{\sigma}_{\text{poly}}$	10[MPa]
p_{tran}	0.55[-]

References

1. Nannan Guo, Ming C. Leu, Additive manufacturing: technology, applications and research needs, *Frontiers of Mechanical Engineering*, **8(3)**, 215-243 (2013)
2. Wei Gao, Yunbo Zhang, Devarajan Ramanujan and et al., The status, challenges, and future of additive manufacturing in engineering, *Computer-Aided Design*, **69**, 65-89 (2015)
3. Jiangtao We, Zeang Zhao, Craig M. Hamel and et al., Evolution of material properties during free radical photopolymerization, *Journal of the Mechanics and Physics of Solids*, **112**, 25-49 (2018)
4. Wentao Yan, Stephen Lin, Orion L. Kafka and et al., Modeling process-structure-property relationships for additive manufacturing, *Frontiers of Mechanical Engineering*, **13(4)**, 482-492, (2018)
5. Trisha Sain, Kaspar Loeffel, Shawn Chester, A thermo-chemo-mechanically coupled constitutive model for curing of glassy polymers, *Journal of the Mechanics and Physics of Solids*, **116**, 267-289, (2018)
6. Christopher N. Bowman and Christopher J. Kloxin, Toward an enhanced understanding and implementation of photopolymerization reaction, *Reactors, Kinetics, and Catalysis*, **Vol. 54, No. 11**, 2775-2795 (2008)
7. Dimitris S. Achilias, A review of modeling of diffusion controlled polymerization reactions, *Macromolecular Theory and Simulations*, **16**, 319-347 (2007)
8. Michael D. Goodner and Christopher N. Bowman, Development of a comprehensive free radical photopolymerization model incorporating heat and

mass transfer effects in thick films, *Chemical Engineering Science*, **57**, 887-900 (2002)
9. Jim H. Lee, Robert K. Prud'homme and Ilhan A. Aksay, Cure depth in photopolymerization: experiments and theory, *Journal of Materials Research,* **Vol. 16, No. 12**, 3536-3543 (2001)